

Measuring an interaction-induced topological phase transition via the single-particle density matrixJun-Hui Zheng^{1,2}, Bernhard Irsigler,¹ Lijia Jiang,³ Christof Weitenberg,^{4,5} and Walter Hofstetter¹¹*Institut für Theoretische Physik, Goethe-Universität, 60438 Frankfurt am Main, Germany*²*Center for Quantum Spintronics, Department of Physics, Norwegian University of Science and Technology, NO-7491 Trondheim, Norway*³*Frankfurt Institute for Advanced Studies, 60438 Frankfurt am Main, Germany*⁴*Institut für Laserphysik, Universität Hamburg, Luruper Chaussee 149, 22761 Hamburg, Germany*⁵*Hamburg Centre for Ultrafast Imaging, Luruper Chaussee 149, 22761 Hamburg, Germany*

(Received 4 January 2020; published 24 January 2020)

Interaction-induced topologically nontrivial phases have been theoretically predicted and need more experimental verification. Cold atom systems with tunable interaction strength provide a flexible platform for studying these effects. Here, we focus on the experimental signature of topological phase and topological phase transition (TPT). Since the topological Hamiltonian carries the information of the topology of the system, we first establish its relation to the single-particle density matrix (SPDM) for interacting two-band systems, and then design a tomography scheme for the SPDM in cold atom experiments. Thus the Berry curvature of the topological Hamiltonian, the Chern number, and the TPT point can be reconstructed from experimental data.

DOI: [10.1103/PhysRevA.101.013631](https://doi.org/10.1103/PhysRevA.101.013631)**I. INTRODUCTION**

Topological insulators are fascinating phases without a local order parameter [1,2]. They have been observed in solid-state materials [3], but also have been realized in quantum simulators such as photonic waveguides [4] and ultracold atoms [5–7]. For two-dimensional noninteracting Chern insulators, the topology can be captured by the Chern number (CN), which is the sum of the integral of the Berry curvature in the Brillouin zone over all occupied bands [2]. Topological insulators, which are characterized by a nonzero Chern number, possess robust conducting edge states at their boundaries. The number of edge states is equal to the CN, according to the bulk-edge correspondence [1]. Experimentally, the topology is often revealed via Hall drift [7,8], robust edge states [4,9,10], Aharonov-Bohm interferometry [11], and Thouless pumping [12,13]. In quantum gas experiments, also the Berry curvature can be reconstructed from quench dynamics [6].

Generalized to interacting systems, the CN has been developed based on the many-body wave function [14] and the single-particle Green's function [15–25], respectively. The former well reflects the number of chiral edge states and the integer or fractional quantum Hall effects. The latter still reflects the number of quasiparticle edge states when the interaction is weak or moderate, but this bulk-edge correspondence can break down in some situations with strong interactions [17–19]. Numerical simulations found that interaction could induce topologically nontrivial phases for specific systems, for example, by band inversion [26–31] or by spontaneous symmetry breaking [32,33]. However, these predictions have so far not been confirmed experimentally except fractional quantum Hall effect. In contrast to solid-state physics, cold atom systems with tunable interaction strength in certain regimes provide a flexible platform for studying interaction effects.

In cold atom systems, the edge states become observable by creating a boundary in the center of the system [30]. Measurement of the Berry curvature could further guarantee the robustness of these edge states and confirm the bulk-edge correspondence. As for the Hall drift measurement developed in Refs. [7,8], it is still unclear how well this semiclassical picture works in the interacting system. For interacting systems, it has been proven that the noninteracting topological Hamiltonian, i.e., the inverse of the zero-frequency Green's function, $H_t \equiv -1/G_{\mathbf{k},i\omega=0}$, carries the information on the topology of the interacting system [20]. Extracting the Berry curvature of the topological Hamiltonian becomes crucial.

In this paper, we consider the half-filled two-band model with repulsive interaction. We illustrate that the Berry curvature of the topological Hamiltonian, the CN, and the topological phase transition (TPT) point can be extracted from the single-particle density matrix (SPDM) of the interacting system in Sec. II, when the quasiparticle lifetime is much smaller than the quasiparticle energy. The spinful Haldane model with on-site interaction is studied and lifetimes of the quasiparticles are evaluated based on Fermi's "golden rule." We confirm the lifetime is much smaller than the quasiparticle energy for weak to moderate interaction. Furthermore, we develop a scheme of tomography for the SPDM of interacting fermions in two-dimensional optical lattices with a two-sublattice structure in Sec. III. This scheme involves time-of-flight (TOF) imaging of the momentum distribution following different sudden quenches, which can be implemented in cold atom experiments. Our method generalizes the scheme of tomographic measurement of pure or mixed states proposed in Refs. [34–36] and realized in Ref. [6].

II. EXTRACTING THE TOPOLOGICAL HAMILTONIAN FROM THE SPDM

The topological Hamiltonian carries the full information on the topology of the interacting system and is theoretically

important for understanding the topological phase transition via analogy with the noninteracting system [20], yet it is not a physical observable. The following statement builds a link between the topological Hamiltonian and the SPDM for half-filled fermionic two-band systems.

If the intrinsic quasiparticle linewidths $\gamma_p(\mathbf{k})$ and $\gamma_h(\mathbf{k})$ are much smaller than the quasiparticle energy [$\epsilon_p(\mathbf{k}) > 0$] and the quasihole energy [$\epsilon_h(\mathbf{k}) < 0$], respectively, i.e., $\gamma_p(\mathbf{k}) \ll |\epsilon_p(\mathbf{k})|$ and $\gamma_h(\mathbf{k}) \ll |\epsilon_h(\mathbf{k})|$, then the inverse of the topological Hamiltonian can be approximated as

$$H_t^{-1}(\mathbf{k}) \simeq \frac{\rho_{\mathbf{k}}^T}{\epsilon_h(\mathbf{k})} + \frac{\mathbf{1} - \rho_{\mathbf{k}}^T}{\epsilon_p(\mathbf{k})}, \quad (1)$$

where $\rho_{\mathbf{k}}^T$ is the transpose of the SPDM and $\mathbf{1}$ is the 2×2 identity matrix. The elements of the SPDM are $\rho_{\mathbf{k},\alpha\beta} = \langle \hat{c}_{\mathbf{k}\alpha}^\dagger \hat{c}_{\mathbf{k}\beta} \rangle$, where $\hat{c}_{\mathbf{k}\alpha}^\dagger$ and $\hat{c}_{\mathbf{k}\beta}$ are the fermionic creation and annihilation operators with momentum \mathbf{k} , and α and β represent the pseudospin.

In order to prove this, we start from the Lehmann representation of the Green's function at zero temperature:

$$\mathcal{G}_{\mathbf{k},i\omega}^{\alpha\beta} = \sum_{\eta} \left[\frac{\langle 0 | \hat{c}_{\mathbf{k}\alpha} | \eta \rangle \langle \eta | \hat{c}_{\mathbf{k}\beta}^\dagger | 0 \rangle}{i\omega - E_{\eta}} + \frac{\langle \bar{\eta} | \hat{c}_{\mathbf{k}\alpha} | 0 \rangle \langle 0 | \hat{c}_{\mathbf{k}\beta}^\dagger | \bar{\eta} \rangle}{i\omega + E_{\bar{\eta}}} \right], \quad (2)$$

where $|0\rangle$ is the many-body ground state with zero energy. η and $\bar{\eta}$ refer to the excitations ($E_{\eta}, E_{\bar{\eta}} > 0$). For each given momentum, the spectral density is given by the imaginary part of the trace of the retarded Green's function, $\varrho_{\mathbf{k}}(\omega) = \sum_{\eta} \eta [|\langle 0 | \hat{c}_{\mathbf{k}\alpha} | \eta \rangle|^2 \delta(\omega - E_{\eta}) + |\langle \bar{\eta} | \hat{c}_{\mathbf{k}\alpha} | 0 \rangle|^2 \delta(\omega + E_{\bar{\eta}})]$. The coefficient $|\langle 0 | \hat{c}_{\mathbf{k}\alpha} | \eta \rangle|^2$ or $|\langle \bar{\eta} | \hat{c}_{\mathbf{k}\alpha} | 0 \rangle|^2$ becomes a non-negligible contribution only when the energy of the many-body state is near to the quasiparticle energy, i.e., $|E_{\eta} - \epsilon_p| \lesssim O[\gamma_p]$ or $|E_{\bar{\eta}} + \epsilon_h| \lesssim O[\gamma_h]$. When the linewidth is rather small compared to the quasiparticle energy, we have $1/E_{\eta} \simeq 1/\epsilon_p$ and $1/E_{\bar{\eta}} \simeq -1/\epsilon_h$ for the contribution to $\varrho_{\mathbf{k}}$ and $\mathcal{G}_{\mathbf{k},i\omega=0}^{\alpha\beta}$. By using $\langle 0 | \hat{c}_{\mathbf{k}\beta}^\dagger \hat{c}_{\mathbf{k}\alpha} | 0 \rangle = \rho_{\mathbf{k},\beta\alpha}$ and $[\hat{c}_{\mathbf{k}\alpha}, \hat{c}_{\mathbf{k}\beta}^\dagger] = \delta_{\alpha\beta}$, we indeed obtain Eq. (1) from Eq. (2) at zero frequency. The error for this approximation is of order $\gamma_{p(h)}/\epsilon_{p(h)}$.

Equation (1) shows that $H_t(\mathbf{k})$ and $\rho_{\mathbf{k}}^T$ have exactly the same eigenvectors and the lower band of the former is mapped onto the higher band of the latter. This allows us to obtain the Berry curvature of the topological Hamiltonian through measuring the SPDM. In addition, Eq. (1) still holds when the temperature T is finite but much smaller than the gap. The additional error is suppressed exponentially by $\exp[-|\epsilon_{p(h)}|/k_B T]$.

A. Interacting Haldane model

Let us consider the spin- $\frac{1}{2}$ Haldane model in a hexagonal optical lattice, which has been realized as a Floquet system in cold atom experiments [6,7]. The Hamiltonian reads

$$\hat{H}_0 = -t \sum_{\langle ij \rangle s} \hat{c}_{is}^\dagger \hat{c}_{js} + \lambda \sum_{\langle\langle ij \rangle\rangle s} e^{i\phi v_{ij}} \hat{c}_{is}^\dagger \hat{c}_{js} + m \sum_{is} \xi_i \hat{c}_{is}^\dagger \hat{c}_{is}, \quad (3)$$

where the first and second terms are the nearest- and the next-nearest-neighbor hopping terms. s refers to spin \uparrow and \downarrow . $v_{ij} = \pm 1$, which is related to the hopping path. In the

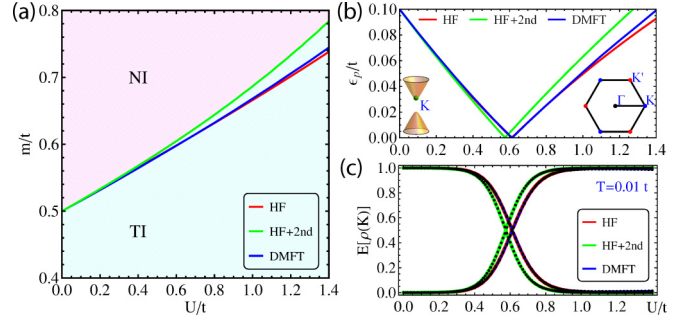


FIG. 1. (a) The phase diagram. (b) The quasiparticle energy of the upper band at the Dirac point (K). (c) The eigenvalues of the SPDM at the K point for $T = 0.01t$. For (b) and (c), $m = 0.6t$.

following, we restrict ourselves to the case of $\phi = \pi/2$, which maximally breaks time-reversal symmetry. The third term is a staggered potential with $\xi_i = 1$ for sublattice A and $\xi_i = -1$ for sublattice B. The system displays a transition into a normal insulator from the quantum Hall phase when $|m|$ becomes larger than $3\sqrt{3}|\lambda|$. The energy gap of the system is $2|m - 3\sqrt{3}\lambda|$ for $m, \lambda > 0$. The on-site interaction reads

$$\hat{H}_{\text{int}} = U \sum_i \hat{n}_{i\uparrow} \hat{n}_{i\downarrow}. \quad (4)$$

The system has $SU(2)$ symmetry in spin space. Note that an interacting Floquet system contains additional subtleties such as micromotion corrections to the interaction [37]. With our static effective model given by Eqs. (3) and (4), we focus on the high-frequency regime, where these corrections are suppressed [38]. Related interaction effects in static models can be found in Refs. [39–42].

For interaction $U \in [0, 1.4t]$, using the Hartree-Fock (HF) approximation, HF plus the second-order perturbation correction (HF+2nd), and dynamical mean-field theory (DMFT), respectively, we plot the phase diagram in Fig. 1(a) for the case $3\sqrt{3}\lambda = 0.5t$. The HF approximation yields a renormalized staggered potential, $m \rightarrow m + \frac{U}{2} [\langle \hat{n}_{A\downarrow} \rangle - \langle \hat{n}_{B\downarrow} \rangle]$, where $\hat{n}_{A(B)\downarrow}$ is the number operator of spin down at each site of sublattice A(B). The repulsive interaction effectively smoothes the staggered potential, and induces the topological insulator phase, which is consistent with the result shown in Ref. [41]. The DMFT further corrects the onsite self-energy slightly. In contrast, the HF+2nd contains corrections for all hopping terms, which are omitted in both HF approximation and DMFT. For $m = 0.6t$, we show the quasiparticle energy at the Dirac point K for different approximations in Fig. 1(b). The gap of the system is exactly twice this energy due to particle-hole symmetry. The interaction closes the gap and inverts the bands at $U \simeq 0.6t$.

B. Lifetime of the quasiparticles

In the following, we confirm that the linewidth $\gamma_{\mathbf{k}}$ is rather small for this interaction regime. The linewidth of a HF quasiparticle excitation (corresponding to the HF approximation) can be obtained by considering all collision channels with one particle from the lower band [see Fig. 2(a)]. Using Fermi's "golden rule," we obtain the linewidth for the quasiparticle

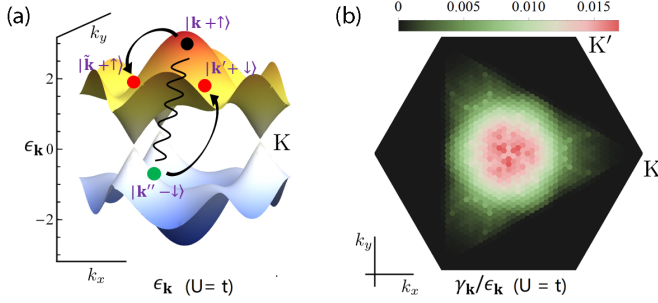


FIG. 2. (a) The HF quasiparticle spectrum and the sketch of the collision between two HF states, and (b) the ratio of the linewidth to the quasiparticle energy. The region where the linewidth vanishes is due to energy and momentum conservation.

state $|\mathbf{k} + \uparrow\rangle$:

$$\gamma_{\mathbf{k}} = 2\pi \times \frac{A_r^2}{(2\pi)^4} \int d^2\mathbf{k}' d^2\mathbf{k}'' \delta(\epsilon_{\mathbf{k}} - \epsilon_{\mathbf{k}'} + \epsilon_{\mathbf{k}''} - \epsilon_{\tilde{\mathbf{k}}}) \times |(\tilde{\mathbf{k}} + \uparrow, \mathbf{k}' + \downarrow | \hat{H}_{\text{int}} | \mathbf{k} + \uparrow, \mathbf{k}'' - \downarrow)|^2, \quad (5)$$

where A_r is the area of the system and $|\mathbf{k} \pm \uparrow\rangle$ is the eigenstate of the higher (lower) band with spin up within the HF approximation. Each energy level is twofold spin degenerate. The two outgoing particles occupy states in the higher band, since the lower band is filled. Momentum conservation demands $\tilde{\mathbf{k}} = \mathbf{k}'' + \mathbf{k} - \mathbf{k}'$. The δ function in Eq. (5) stems from energy conservation. The phase space of the final states is constrained by momentum and energy conservation. In particular, for the quasiparticle at the Dirac point \mathbf{K} the linewidth vanishes for zero temperature, since all collision channels are forbidden. In comparison, a quasiparticle excitation with a higher energy has a larger linewidth and ratio $\gamma_{\mathbf{k}}/\epsilon_{\mathbf{k}}$ due to a larger phase space of the final states [see Fig. 2(b)]. The linewidth as a function of interaction strength, Eq. (5), can formally be parametrized as $c_1 U^2(1 + c_2 U + \dots)$, where the first U^2 directly arises from \hat{H}_{int} and the part $c_2 U$ is due to the interaction-dependent HF states. For weak interaction, the linewidth increases quadratically as a function of the interaction strength. In Fig. 2, we show the HF quasiparticle energy and the ratio of the linewidth to the energy for $U = t$. For different interaction strengths, the linewidth has a similar profile in momentum space but with an interaction-dependent rescaling. A large interaction enhances the linewidth, and thus the ratio $\gamma_{\mathbf{k}}/\epsilon_{\mathbf{k}}$. We find that up to $U = t$ the linewidth is still rather small compared to the energy ($< 2.6\%$) for $m \in [0, t]$. A similar conclusion can be drawn for quasihole states. This confirms the validity of the approximation (1).

The ratio $\gamma_{\mathbf{k}}/\epsilon_{\mathbf{k}}$ also reflects how much the quasiparticle differs from a single-particle pure state. In principle, when the interaction becomes stronger, the deviation increases. On the other hand, also the temperature T can mix states. For $T = 0.01t$, we plot the eigenvalues of the SPDM within HF and HF+2nd approximation, respectively, for the \mathbf{K} point in Fig. 1(c). The position of the gap closing of the SPDM almost coincides with that of the energy in Fig. 1(b). This means that the topological phase transition point can be obtained from the gap closing point of the SPDM as expected. The small

deviation from the real phase transition point stems from finite T and linewidth at the Γ point, respectively.

III. TOMOGRAPHY FOR THE SPDM

We have shown that the higher band of $\rho_{\mathbf{k}}^T$ provides information on topological properties of the lower-energy band of the system. In the following, we illustrate how to measure it in cold atom experiments. Including finite temperature and interaction effects, the many-body density matrix of an interacting system is $\mathcal{P}_M = \sum_{\eta} p_{\eta} |\eta\rangle\langle\eta|$, where $|\eta\rangle$ is a many-body energy eigenstate and p_{η} is the thermal equilibrium probability distribution function with the constraint $\sum_{\eta} p_{\eta} = 1$. The SPDM becomes $\rho_{\mathbf{k},\alpha\beta} = \text{Tr}[\hat{c}_{\mathbf{k}\alpha}^{\dagger} \hat{c}_{\mathbf{k}\beta} \mathcal{P}_M]$. Here and in the following, the spin index is dropped due to SU(2) symmetry. α and β are the pseudospin sublattice indices (A, B). The transpose of the SPDM can be represented as

$$\rho_{\mathbf{k}}^T = \frac{1}{2} \sum_{i=0}^3 a_{\mathbf{k},i} \sigma_i, \quad (6)$$

where $\sigma_{1(2,3)}$ is the Pauli matrix and $\sigma_0 = \mathbf{1}$. The coefficients are $a_{\mathbf{k},i} = \text{Tr}[\rho_{\mathbf{k}}^T \sigma_i] = \sum_{\eta} p_{\eta} \langle\eta| \hat{c}_{\mathbf{k}\alpha}^{\dagger} \sigma_i \hat{c}_{\mathbf{k}\beta} |\eta\rangle$, where $\hat{c}_{\mathbf{k}} = (\hat{c}_{\mathbf{k}A}, \hat{c}_{\mathbf{k}B})^T$. Note that $a_{\mathbf{k},0} > 0$ is the total density $\rho_{\mathbf{k},AA} + \rho_{\mathbf{k},BB}$, and it equals 1 for the half-filling case with particle-hole symmetry.

Quench dynamics can be used to reconstruct the vector $\mathbf{a}_{\mathbf{k}} \equiv (a_{\mathbf{k},1}, a_{\mathbf{k},2}, a_{\mathbf{k},3})$. Let us suppose that the system is suddenly quenched to a new noninteracting Hamiltonian $\hat{\mathcal{H}} = \frac{\Omega}{2} \sum_{\mathbf{k}} \hat{c}_{\mathbf{k}}^{\dagger} \boldsymbol{\sigma} \cdot \mathbf{d}_{\mathbf{k}} \hat{c}_{\mathbf{k}}$ at the time $\tau = 0$, where $\mathbf{d}_{\mathbf{k}}$ is a momentum-dependent unit vector. The coefficients of $\rho_{\mathbf{k}}^T(\tau)$ become $a_{\mathbf{k},j}(\tau) = \sum_{\eta} p_{\eta} \langle\eta| \hat{c}_{\mathbf{k}\alpha}^{\dagger} V_{\mathbf{k}}^{\dagger}(\tau) \sigma_j V_{\mathbf{k}}(\tau) \hat{c}_{\mathbf{k}\beta} |\eta\rangle$ after evolution to time $\tau > 0$, where $V_{\mathbf{k}}(\tau) = e^{-i\tau(\Omega/2)\boldsymbol{\sigma} \cdot \mathbf{d}_{\mathbf{k}}}$ is a 2×2 matrix. Since $V_{\mathbf{k}}^{\dagger}(\tau) \sigma_j V_{\mathbf{k}}(\tau)$ is a linear combination of σ_i , this formula links the coefficients at time τ to those at time $\tau = 0$. The evolution effectively rotates the vector $\mathbf{a}_{\mathbf{k}}$, and $a_{\mathbf{k},0}$ is time independent after the quench. Thus, the initial SPDM can be deduced from the final coefficients. However, in TOF experiments, not all of the final coefficients can be recorded. The density operator of particles in momentum space observed in TOF experiments is $\hat{N}_{\text{TOF}}(\mathbf{k}) \simeq |\tilde{w}(\mathbf{k})|^2 \sum_{\mathbf{R}, \mathbf{R}'} e^{-i\mathbf{k} \cdot (\mathbf{R} - \mathbf{R}')} \hat{c}_{\mathbf{R}}^{\dagger} \hat{c}_{\mathbf{R}}$, where \mathbf{R} and \mathbf{R}' denote lattice sites and $\tilde{w}(\mathbf{k})$ is the Fourier transformation of the Wannier function [43]. So the particle density observed is

$$N_{\text{TOF}}(\mathbf{k}) \simeq |\tilde{w}(\mathbf{k})|^2 ((\hat{c}_{\mathbf{k}A}^{\dagger} + \hat{c}_{\mathbf{k}B}^{\dagger})(\hat{c}_{\mathbf{k}A} + \hat{c}_{\mathbf{k}B})) = |\tilde{w}(\mathbf{k})|^2 [a_{\mathbf{k},0}^F + a_{\mathbf{k},1}^F], \quad (7)$$

where $a_{\mathbf{k},0}^F = a_{\mathbf{k},0} = 1$ and $a_{\mathbf{k},1}^F$ are the components of the final SPDM at the time before the free expansion. Only the component $a_{\mathbf{k},1}^F$ can be detected.

Through rotating the initial vector $\mathbf{a}_{\mathbf{k}}$ during the dynamics after the quench, we can reconstruct $\mathbf{a}_{\mathbf{k}}$ by detecting its projection onto the first component. In the first protocol, the system is suddenly quenched to $\hat{\mathcal{H}}$ with $\mathbf{d}_{\mathbf{k}} = (0, 0, 1)$ at the time $\tau = 0$, which can be realized by switching off all tunneling and interaction but with the staggered potential $\Omega/2$ remaining [34]. The rotation couples $a_{\mathbf{k},1}$ and $a_{\mathbf{k},2}$, and we have $a_{\mathbf{k},1}(\tau) = \cos(\Omega\tau)a_{\mathbf{k},1} - \sin(\Omega\tau)a_{\mathbf{k},2}$. If the atoms are completely released at time τ , then the particle density

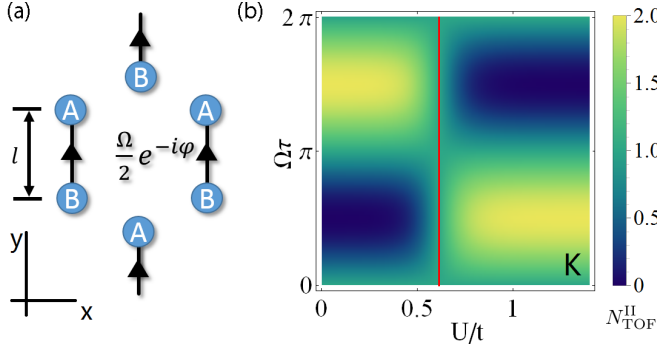


FIG. 3. (a) Second quench protocol and (b) particle density oscillation observed in TOF experiment for the Dirac point $\mathbf{k} = (4\pi/3\sqrt{3}l, 0)$, by using the second protocol with $\varphi = \pi/2$. The red line represents the phase transition. $T = 0.01t$.

observed by TOF imaging is

$$N_{\text{TOF}}^I(\mathbf{k}, \tau) \propto 1 + \cos(\Omega\tau)a_{\mathbf{k},1} - \sin(\Omega\tau)a_{\mathbf{k},2}. \quad (8)$$

The protocol is the same as that for a single-particle pure state (SPPS) in noninteracting systems [34]. By fitting to the experimental data, both $a_{\mathbf{k},1}$ and $a_{\mathbf{k},2}$ can be obtained from the oscillating behavior of $N_{\text{TOF}}^I(\mathbf{k}, \tau)$. For the SPPS, $|\mathbf{a}_{\mathbf{k}}| = 1$ so that $|a_{\mathbf{k},3}|$ can be obtained from the known $a_{\mathbf{k},1}$ and $a_{\mathbf{k},2}$. This is not true for a general density matrix where $|\mathbf{a}_{\mathbf{k}}| \leq 1$. Additional experiments involving components $a_{\mathbf{k},1}$ and $a_{\mathbf{k},3}$ are needed for detecting $a_{\mathbf{k},3}$.

The second protocol uses the quench channel \hat{H} with $\mathbf{d}(\mathbf{k}) = (\cos(k_y l + \varphi), \sin(k_y l + \varphi), 0)$, where l is the lattice constant. This Hamiltonian can be realized by switching on tunneling $\Omega e^{-i\varphi}/2$ between A-B sublattices only along the y direction, as shown in Fig. 3(a). This Hamiltonian induces a similar precession dynamics on the Bloch sphere as the first protocol, but now along a vector, which lies in the xy plane. The coefficient then becomes

$$\begin{aligned} a_{\mathbf{k},1}(\tau) = & [\cos^2(\Omega\tau/2) + \sin^2(\Omega\tau/2) \cos(2k_y l + 2\varphi)]a_{\mathbf{k},1} \\ & + \sin^2(\Omega\tau/2) \sin(2k_y l + 2\varphi)a_{\mathbf{k},2} \\ & + \sin(\Omega\tau) \sin(k_y l + \varphi)a_{\mathbf{k},3}. \end{aligned} \quad (9)$$

Using known $a_{\mathbf{k},1}$ and $a_{\mathbf{k},2}$, we can get $a_{\mathbf{k},3}$ by detecting the particle density $N_{\text{TOF}}^{II}(\mathbf{k}, \tau) \propto 1 + a_{\mathbf{k},1}(\tau)$, except for the points \mathbf{k} with $\sin(k_y l + \varphi) = 0$. At these points, $\mathbf{d}(\mathbf{k}) = (1, 0, 0)$, which cannot generate an effective rotation that couples $a_{\mathbf{k},1}$ and $a_{\mathbf{k},3}$. To obtain $a_{\mathbf{k},3}$ in the whole Brillouin zone, a similar experiment with $\varphi \rightarrow \varphi - \pi/2$ can be implemented. One can choose the two experiments with $\varphi = \pi$ (normal tunneling) and $\varphi = \pi/2$, respectively. Since the second protocol directly accesses $a_{\mathbf{k},3}$, there is no missing information on the northern or southern hemisphere as it appears for the quench on flat bands [34].

Note that all the different Hamiltonians discussed above could be realized by starting with a static lattice with large AB offset and shaking [6,44]. Specifically, circular shaking is used for simulating the Haldane model, while asymmetric linear shaking along the y direction can be used for

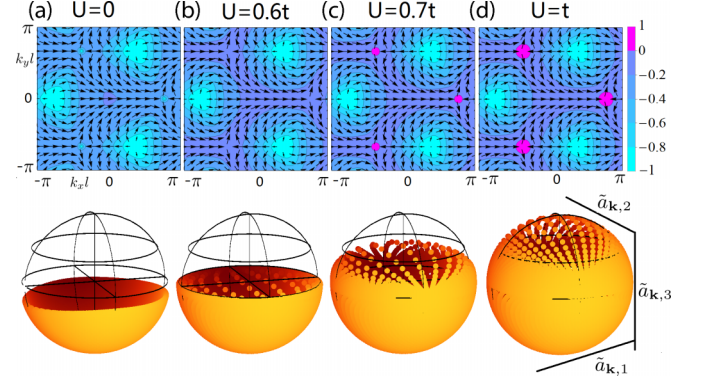


FIG. 4. Upper: Vector plot of $(\tilde{a}_{\mathbf{k},1}, \tilde{a}_{\mathbf{k},2})$ and density plot of $\tilde{a}_{\mathbf{k},3}$. Bottom: 3D plot of $\tilde{\mathbf{a}}_{\mathbf{k}}$. $T = 0.01t$.

realizing the situation in Fig. 3(a) [45]. For realizing the first protocol, the quench can simply be realized by switching off the shaking, which was used to realize the Haldane model before the quench. The interaction can be switched off by using a Feshbach resonance [46] or by tuning the confinement strength along the z direction for a transverse confinement optical lattice. The time scale for ramping the interaction to zero should be much smaller than the time scale $1/\Omega$ and $1/U$, so that interaction effects during quench dynamics can be omitted.

The Berry curvature can then be extracted from the known $\mathbf{a}_{\mathbf{k}}$. Note that in the Fourier-transformed basis, $\hat{c}_{\mathbf{k}A(B)} \propto \sum_{\mathbf{R} \in A(B)} \hat{c}_{\mathbf{R}} e^{-i\mathbf{k} \cdot \mathbf{R}}$, the Hamiltonian is not periodic but with an additional unitary transformation after translating by a reciprocal-lattice vector \mathbf{Q} . We obtain $h(\mathbf{k} + \mathbf{Q}) = U_{\mathbf{Q}}^\dagger h(\mathbf{k}) U_{\mathbf{Q}}$, where $U_{\mathbf{Q}} = \text{diag}(1, e^{-iQ_y l})$ and $h(\mathbf{k})$ is the matrix representation of the noninteracting Hamiltonian \hat{H}_0 . Thus we introduce the unitary transformation $(\hat{c}_{\mathbf{k}A}, \hat{c}_{\mathbf{k}B}) = (\hat{c}_{\mathbf{k}A}, \hat{c}_{\mathbf{k}B} e^{-ik_y l})$ to render the Hamiltonian periodic. The components for the periodic SPDM $\langle \hat{c}_{\mathbf{k}\alpha}^\dagger \hat{c}_{\mathbf{k}\beta} \rangle$ are $\tilde{\mathbf{a}}_{\mathbf{k}} = (\cos(k_y l)a_{\mathbf{k},1} + \sin(k_y l)a_{\mathbf{k},2}, \cos(k_y l)a_{\mathbf{k},2} - \sin(k_y l)a_{\mathbf{k},1}, a_{\mathbf{k},3})$. We plot the result of $\tilde{\mathbf{a}}_{\mathbf{k}}$ for different interaction strengths in Fig. 4. The two-dimensional vector $(\tilde{a}_{\mathbf{k},1}, \tilde{a}_{\mathbf{k},2})$ has an opposite winding behavior circuiting the Dirac points \mathbf{K} and \mathbf{K}' , as in noninteracting systems [34]. The third component $\tilde{a}_{\mathbf{k},3}$ for the \mathbf{K} point moves from the south pole to the north pole when increasing the interaction strength. It changes its sign when $U \simeq 0.6t$. The vector $\tilde{\mathbf{a}}_{\mathbf{k}}$ maps the Brillouin zone to a closed curved surface in three-dimensional space. For the noninteracting case, it looks like a deflated ball. Interaction inflates this ball to be round. The condition for a topological phase of the higher (and lower) band of $\rho_{\mathbf{k}}^T$ is that the origin is enclosed by that surface [2]. This coincides with whether $a_{\mathbf{k},3}$ at the \mathbf{K} point is positive. Recall that for a single-particle pure state $|\mathbf{a}_{\mathbf{k}}| = 1$ and it lives on the surface of the sphere [see Fig. 4(a)]. With interaction and finite temperature, $\mathbf{a}_{\mathbf{k}}$ can lie within the sphere and the topological phase transition occurs mildly. The Berry curvature of the higher band of $\rho_{\mathbf{k}}^T$ can be obtained by using the formula $-\frac{1}{4\pi} (\partial_{k_x} \hat{\mathbf{a}} \times \partial_{k_y} \hat{\mathbf{a}}) \cdot \hat{\mathbf{a}}$, where $\hat{\mathbf{a}} = \tilde{\mathbf{a}}/|\tilde{\mathbf{a}}|$. Its integral gives the the CN.

To determine the phase transition point, we use the second protocol with $\varphi = \pi/2$. For the \mathbf{K} point with momentum

$\mathbf{k} = (4\pi/3\sqrt{3}l, 0)$, the particle density observed becomes

$$N_{\text{TOF}}^{\text{II}}(\mathbf{k}, \tau) \propto 1 + \cos(\Omega\tau)a_{\mathbf{k},1} + \sin(\Omega\tau)a_{\mathbf{k},3}. \quad (10)$$

For the K point, $a_{\mathbf{k},1}$ is very small, and thus $N_{\text{TOF}}^{\text{II}}$ gets a π -phase shift when $a_{\mathbf{k},3}$ changes sign. This is shown in Fig. 3(b). The point of sign change is exactly the phase transition point.

In conclusion, we have established a link between the SPDM and the topological Hamiltonian, and propose a scheme for detecting the SPDM in experiments. The scheme generalizes the tomographic measurement of pure or mixed states proposed in Refs. [34–36]. It should be experimentally achievable by using well-developed techniques [6]. This opens up the possibility to experimentally measure the topological phenomena in the interacting ultracold atom systems. The scheme for measuring the SPDM proposed here can be applied to other A-B sublattice structures. Without particle-hole symmetry, only the rescaled vector $\mathbf{a}_{\mathbf{k}}/a_{\mathbf{k},0}$ can be obtained by fitting to the experiment. However, this rescaled vector already contains the full topological information of

the system. For very strong interaction, where the quasiparticle picture does not hold anymore, the connection between the topological Hamiltonian and the SPDM is still an open question. Moreover, the bulk-edge correspondence may break down in this regime. From the aspect of the topological Hamiltonian, it means there is a band crossing at the infinite energy. Thus, the CN of the bands of the topological Hamiltonian is changed without a band inversion at zero energy. A generalized scheme for systems with more bands (especially if more than one band is occupied) will be the subject of future research.

ACKNOWLEDGMENTS

J.-H.Z. acknowledges useful discussions with Andrew Hayward, Fabian Heidrich-Meisner, and Oleksandr Tsypliyatyev. This research was funded by the Deutsche Forschungsgemeinschaft (DFG, German Research Foundation) via Research Unit FOR 2414 under Project No. 277974659. This work was also supported by the DFG via the high-performance computing center LOEWE-CSC.

-
- [1] M. Z. Hasan and C. L. Kane, *Rev. Mod. Phys.* **82**, 3045 (2010).
 - [2] D. Xiao, M.-C. Chang, and Q. Niu, *Rev. Mod. Phys.* **82**, 1959 (2010).
 - [3] P. Gehring, H. M. Benia, Y. Weng, R. Dinnebier, C. R. Ast, M. Burghard, and K. Kern, *Nano Lett.* **13**, 1179 (2013).
 - [4] M. C. Rechtsman, Y. Plotnik, J. M. Zeuner, D. Song, Z. Chen, A. Szameit, and M. Segev, *Phys. Rev. Lett.* **111**, 103901 (2013).
 - [5] M. Aidelsburger, M. Atala, M. Lohse, J. T. Barreiro, B. Paredes, and I. Bloch, *Phys. Rev. Lett.* **111**, 185301 (2013).
 - [6] N. Fläschner, B. S. Rem, M. Tarnowski, D. Vogel, D.-S. Lühmann, K. Sengstock, and C. Weitenberg, *Science* **352**, 1091 (2016).
 - [7] G. Jotzu, M. Messer, R. Desbuquois, M. Lebrat, T. Uehlinger, D. Greif, and T. Esslinger, *Nature (London)* **515**, 237 (2014).
 - [8] M. Aidelsburger, M. Lohse, C. Schweizer, M. Atala, J. T. Barreiro, S. Nascimbéne, N. R. Cooper, I. Bloch, and N. Goldman, *Nat. Phys.* **11**, 162 (2015).
 - [9] M. Mancini, G. Pagano, G. Cappellini, L. Livi, M. Rider, J. Catani, C. Sias, P. Zoller, M. Inguscio, M. Dalmonte, and L. Fallani, *Science* **349**, 1510 (2015).
 - [10] B. K. Stuhl, H.-I. Lu, L. M. Ayccock, D. Genkina, and I. B. Spielman, *Science* **349**, 1514 (2015).
 - [11] L. Duca, T. Li, M. Reitter, I. Bloch, M. Schleier-Smith, and U. Schneider, *Science* **347**, 288 (2015).
 - [12] S. Nakajima, T. Tomita, S. Taie, T. Ichinose, H. Ozawa, L. Wang, M. Troyer, and Y. Takahashi, *Nat. Phys.* **12**, 296 (2016).
 - [13] M. Lohse, C. Schweizer, O. Zilberberg, M. Aidelsburger, and I. Bloch, *Nat. Phys.* **12**, 350 (2016).
 - [14] Q. Niu, D. J. Thouless, and Y.-S. Wu, *Phys. Rev. B* **31**, 3372 (1985).
 - [15] K. Ishikawa and T. Matsuyama, *Z. Phys. C* **33**, 41 (1986); *Nucl. Phys. B* **280**, 523 (1987).
 - [16] Z. Wang, X.-L. Qi, and S.-C. Zhang, *Phys. Rev. Lett.* **105**, 256803 (2010).
 - [17] V. Gurarie, *Phys. Rev. B* **83**, 085426 (2011).
 - [18] Y.-Z. You, Z. Wang, J. Oon, and C. Xu, *Phys. Rev. B* **90**, 060502(R) (2014).
 - [19] Y.-Y. He, H.-Q. Wu, Z. Y. Meng, and Z.-Y. Lu, *Phys. Rev. B* **93**, 195164 (2016).
 - [20] Z. Wang and S.-C. Zhang, *Phys. Rev. X* **2**, 031008 (2012).
 - [21] R. Shindou and L. Balents, *Phys. Rev. Lett.* **97**, 216601 (2006).
 - [22] R. Shindou and L. Balents, *Phys. Rev. B* **77**, 035110 (2008).
 - [23] C. H. Wong and R. A. Duine, *Phys. Rev. A* **88**, 053631 (2013).
 - [24] Y. Li, P. Sengupta, G. G. Batrouni, C. Miniatura, and B. Grémaud, *Phys. Rev. A* **92**, 043605 (2015).
 - [25] J.-H. Zheng and W. Hofstetter, *Phys. Rev. B* **97**, 195434 (2018).
 - [26] D. A. Abanin and D. A. Pesin, *Phys. Rev. Lett.* **109**, 066802 (2012).
 - [27] P. Kumar, T. Mertz, and W. Hofstetter, *Phys. Rev. B* **94**, 115161 (2016).
 - [28] W. Hofstetter and T. Qin, *J. Phys. B* **51**, 082001 (2018).
 - [29] S. Rachel, *Rep. Prog. Phys.* **81**, 116501 (2018).
 - [30] B. Irsigler, J.-H. Zheng, and W. Hofstetter, *Phys. Rev. Lett.* **122**, 010406 (2019).
 - [31] J.-H. Zheng, T. Qin, and W. Hofstetter, *Phys. Rev. B* **99**, 125138 (2019).
 - [32] S. Raghu, X.-L. Qi, C. Honerkamp, and S.-C. Zhang, *Phys. Rev. Lett.* **100**, 156401 (2008).
 - [33] W. Zhu, S.-S. Gong, T.-S. Zeng, L. Fu, and D. N. Sheng, *Phys. Rev. Lett.* **117**, 096402 (2016).
 - [34] P. Hauke, M. Lewenstein, and A. Eckardt, *Phys. Rev. Lett.* **113**, 045303 (2014).
 - [35] L. A. P. Ardila, M. Heyl, and A. Eckardt, *Phys. Rev. Lett.* **121**, 260401 (2018).

- [36] M. Tarnowski, M. Nuske, N. Fläschner, B. Rem, D. Vogel, L. Freystatzky, K. Sengstock, L. Mathey, and C. Weitenberg, *Phys. Rev. Lett.* **118**, 240403 (2017).
- [37] E. Anisimovas, G. Žlabys, B. M. Anderson, G. Juzeliūnas, and A. Eckardt, *Phys. Rev. B* **91**, 245135 (2015).
- [38] A. Eckardt, *Rev. Mod. Phys.* **89**, 011004 (2017).
- [39] J. Imriška, L. Wang, and M. Troyer, *Phys. Rev. B* **94**, 035109 (2016).
- [40] J. Wu, J. P. L. Faye, D. Sénéchal, and J. Maciejko, *Phys. Rev. B* **93**, 075131 (2016).
- [41] T. I. Vanhala, T. Siro, L. Liang, M. Troyer, A. Harju, and P. Törmä, *Phys. Rev. Lett.* **116**, 225305 (2016).
- [42] A. Rubio-García and J. J. García-Ripoll, *New J. Phys.* **20**, 043033 (2018).
- [43] I. Bloch, J. Dalibard, and W. Zwerger, *Rev. Mod. Phys.* **80**, 885 (2008).
- [44] M. Tarnowski, F. Nur Únal, N. Fläschner, B. S. Rem, A. Eckardt, K. Sengstock, and C. Weitenberg, *Nat. Commun.* **10**, 1728 (2019).
- [45] J. Struck, C. Ölschläger, M. Weinberg, P. Hauke, J. Simonet, A. Eckardt, M. Lewenstein, K. Sengstock, and P. Windpassinger, *Phys. Rev. Lett.* **108**, 225304 (2012).
- [46] C. Chin, R. Grimm, P. Julienne, and E. Tiesinga, *Rev. Mod. Phys.* **82**, 1225 (2010).